Molecular insights into the reactivity of aquatic natural organic matter towards hydroxyl (•OH) and sulfate (SO4•–) radicals using FT-ICR MS

Suona Zhang, Zhineng Hao, Jingfu Liu, Leo Gutierrez, Jean-Philippe Croué

Molecular insights into the reactivity of aquatic natural organic matter towards hydroxyl (•OH) and sulfate ($SO_4^{\bullet-}$) radicals using FT-ICR MS

Suona Zhang, [†] Zhineng Hao, [§] Jingfu Liu,*[,§] Leo Gutierrez,[&] and Jean-Philippe Croué *[,†,‡]

[†]Curtin Water Quality Research Centre, Department of Chemistry, Curtin University, Perth 6102, Australia

[§] Research Center for Eco-Environmental Sciences, Chinese Academy of Sciences, Beijing 10085, China

[‡] Institut de Chimie des Milieux et des Matériaux IC2MP UMR 7285 CNRS, Université de Poitiers, Poitiers 86000, France

[&] Facultad del Mar y Medio Ambiente, Universidad del Pacifico, Ecuador

Corresponding author:

*jfliu@rcees.ac.cn; Fax: +86-10-62849192

*jean.philippe.croue@univ-poitiers.fr; Tel.: +33 (0) 7 87 09 44 66

Abstract

The higher scavenging capacity of natural organic matter (NOM) to hydroxyl radical ($^{\bullet}OH$) than sulfate radical ($SO_4^{\bullet-}$) has been long-acknowledged. However, the difference in reactivity and the influence of initial characteristics, especially at the molecular-level, remain unaddressed. In this study, the reactivities of different NOM isolates to $^{\bullet}OH$ and $SO_4^{\bullet-}$ were compared based on the determined second-order rate constants following the depletion of UV_{254}-absorbing moieties. Three NOM isolates with varying characteristics were selected to investigate the influence of initial characteristics on their reactivities. With the identified reactive molecules using Fourier transform ion cyclotron resonance mass spectrometry (FT-ICR MS), the distinct reactivity between the radicals and the influence of the initial characteristics were illustrated. The reactivity towards $SO_4^{\bullet-}$ was dominated by the electron density of the molecules (i.e., double bond equivalent (DBE)), while that of $^{\bullet}OH$ was also shaped by molecular size (i.e., *m*/*z*) and composition (i.e., N- or S-incorporation). The examination on the exclusively reactive molecules (accounting for 10-20%) reflected a preferred H-abstraction by $^{\bullet}OH$ and decarboxylation by $SO_4^{\bullet-}$. Moreover, the analysis on the shared reactive molecules (80-90%) based on the UV_{254} versus electron-donating capacity (EDC) dependency revealed a prevalent $^{\bullet}OH$ addition while single electron transfer to $SO_4^{\bullet-}$. The different reaction rates associated with the proposed transformation pathways supported the observed higher reactivity of NOM to $^{\bullet}OH$ than $SO_4^{\bullet-}$.

Keywords: NOM, Hydroxyl radical, Sulfate radical, Influential characteristics, Transformation pathways.

1. Introduction

Hydroxyl radical ($^{\bullet}OH$) or sulfate radical ($SO_4^{\bullet-}$)-based advanced oxidation processes (AOPs) have received considerable research interest worldwide. The vast majority of the studies have focused on the removal of organic micropollutants [1-6], while significantly less attention has been directed to the reactivity of natural organic matter (NOM) [7, 8]. NOM (i.e., the complex and heterogeneous product of decayed biological material) is ubiquitously present and plays multiple critical roles in both engineered and natural aquatic systems [9-18].

According to previous studies, the scavenging capacity of NOM to $^{\bullet}OH$ (~10^4 $(mgC/L)^{-1}\cdot s^{-1}$) is higher than that of $SO_4^{\bullet-}$ (~10^3 $(mgC/L)^{-1}\cdot s^{-1}$) [19, 20]. The reactivity of radical species with NOM depends on the nature and diversity of the reactive sites (i.e., molecules with specific composition and characteristics) and the reaction pathways (e.g., radical addition, electron transfer, or H-abstraction). Generally, the lower reactivity to $SO_4^{\bullet-}$ has been attributed to its high selectivity toward electron-rich moieties and unfavorable/slower reaction with saturated structures (i.e., either through H-abstraction [20] or decarboxylation [21]). Nevertheless, additional research is highly required to clearly describe the difference in reactivity, especially with a focus on the reactive sites at the molecular level. Currently, the characterization of NOM in $^{\bullet}OH$ or $SO_4^{\bullet-}$-based AOPs has been mainly achieved through measurements of specific properties such as electron-donating capacity (EDC), UV light absorbing property (UV_{254}), fluorescent intensity (FI), molecular weight (MW), and total organic content (TOC) [22, 23]. Although these analytical tools provide insight into bulk properties, they prove unsuitable in revealing detailed information at the molecular level.

Ultra-high resolution mass spectroscopy, i.e., Fourier transform ion cyclotron resonance mass spectroscopy (FT-ICR MS), allows the detection of individual molecules within the complex natural organic mixtures based on which exact molecular formulas can be unambiguously assigned). As a result, molecular composition and molecular characteristics can be readily

obtained. This analytical technique has been widely used for the identification of newly-formed disinfection by-products, NOM components adsorbing onto minerals, and molecular characterization of NOM transformation in various processes [8, 24-29] (e.g., coagulation, disinfection, advanced oxidation, biological degradation, or sunlight-induced photochemical reaction). Based on the extensive and successful use of FT-ICR MS in these fields, a molecular-level investigation on the radical-induced reactivity of NOM will advance our fundamental understanding of the preferential molecular target of radicals.

Very recently, the disparate transformation patterns of Suwannee River NOM by $^{\bullet}OH$ and $SO_4^{\bullet-}$ have been demonstrated at molecular-level using Orbitrap mass spectrometer [8]. A distinct transformation of aliphatic components by $^{\bullet}OH$ was observed, while the transformation of aromatic and olefinic structures was the predominant pathway by $SO_4^{\bullet-}$. However, apart from the saturation degree of NOM, its reactivity and transformation should also be defined by other characteristics, i.e., molecular composition, molecular weight, functional groups, etc. Considering the highly heterogeneous nature of NOM, a molecular-level understanding on its reactivity and influential characteristics would be practically meaningful for the application of the radical-based AOPs in water treatment.

To fill the information gap, the reactivity of three NOM isolates extracted from different surface waters towards $^{\bullet}OH$ and $SO_4^{\bullet-}$ (i.e., generated by UV/H_2O_2 and UV/PDS, respectively) was investigated using FT-ICR MS. The NOM samples exhibited varied characteristics (Table S1 and S2) in aromaticity, molecular size, and composition, properly representing a wide spectrum of aquatic environments. The NOM reactivity was firstly explored by calculating the second-order rate constant of the degradation of UV_{254}-absorbing moieties using a modified method as previously reported [23]. Secondly, the reactivity of different NOM samples was further examined through the identification of the reactive molecules susceptible to radical attack. Finally, the reaction pathways associated with the

reactive molecules were discussed based on the identified reactive sites and the analysis of bulk properties (i.e., EDC and UV_{254}).

2. Materials and methods

2.1 Chemicals and NOM samples

Methanol and ethyl acetate of High-Performance Liquid Chromatography (HPLC) grade were purchased from Honeywell Burdick & Jackson. Sulfuric acid (H_2SO_4, 98%) and hydrochloric acid (HCl, 32%) were supplied by UNIVAR. All the solutions: peroxodisulfate (PDS; ⩾98%, Sigma-Aldrich), hydrogen peroxide (H_2O_2, 30%, UNIVAR), *p*-chlorobenzoic acid (*p*CBA, Acros Organics), and nitrobenzene (NB, Sigma-Aldrich), were prepared with ultrapure water.

Three NOM fractions previously isolated from different surface waters were selected: Hydrophobic acid NOM extracted from Suwannee River water (S-HPOA, USA), hydrophobic NOM from Ribou Reservoir NOM (R-HPO, France), and hydrophobic NOM from Colorado River (C-HPO, USA). The basic characteristics of the NOM samples were summarized in Table S1, Supporting Information (SI).

2.2 UV-AOPs experimental procedure

$^{\bullet}OH$ and $SO_4^{\bullet-}$ were generated through UV irradiation of H_2O_2 and PDS in unbuffered solutions, respectively. Buffer was not applied in the study to avoid the potential interference caused by the relevant produced radical species. The UV-AOPs experiments were conducted with an LP-UV collimated beam device (CBD). The detailed information on the UV-CBD and the quantification of radical production were provided in the SI (Fig. S1, Text S1a).

An incident UV intensity of ~0.9 $mW \cdot cm^{-2}$ was applied to a 250 mL NOM-containing (~ 4 $mgC \cdot L^{-1}$) solution in a beaker with a diameter of 84 mm. Oxidants (H_2O_2 or PDS: 1.0 mM, unless otherwise specified) were individually added into the solutions immediately prior to UV irradiation. The initial UV fluence varied among different NOM-containing solutions due

to their difference in UV absorbance at 254 nm, and was calculated as 633, 760, and 886 $mJ \cdot cm^{-2}$ for S-HPOA-, R-HPO-, and C-HPO-containing solutions, respectively. A similar initial pH (~4.65) was recorded for UV/H_2O_2 or UV/PDS experiments. The pH remained relatively stable in the UV/H_2O_2 system; however, it decreased by approximately one pH unit in the UV/PDS system after 30 min of irradiation. Samples for FT-ICR MS analysis were acidified to ~ pH 2 with HCl prior to solid-phase extraction (Text S1b). Another set of experiments using 30 mL solution in a Petri-dish was conducted to investigate the impact of the produced radicals on UV-absorbing and electron-donating moieties (Text S1c).

Complementary experiments were performed under the same experimental conditions as aforementioned in the presence of 1 μM *p*CBA and 1 μM NB as probe compounds for the determination of $^{\bullet}OH$ and $SO_4^{\bullet-}$ steady-state radical concentrations. Samples were collected at specific time intervals for probe measurement with the addition of 1 M methanol as a radical quencher. Overall, the $^{\bullet}OH$ accounted for less than 10% of the radical species produced in the UV/PDS system under all experimental conditions. The change in UV_{254} of the NOM solutions with time was immediately recorded without any quencher application. This recorded value was further corrected by subtracting the absorbance of oxidants and probe compounds and the contribution of sole UV irradiation. Specifically, the residual of oxidant was analysed through modeling [1], and the concentration of probe compounds was measured using HPLC. The absorbance was calculated using Lambert-Beer law. Specifically, the second-order rate constant of NOM was determined by normalizing the degradation rate of UV_{254}-absorbing moieties with steady-state radical concentration. The calculation of the steady-state radical concentration was detailed in Text S1d. The samples collected for TOC measurements were acidified to pH ~2 with H_2SO_4.

2.3 FT-ICR MS analysis

A 15.0 T superconducting magnet equipped with a Bruker SolariX FT-ICR MS was used to collect the ultra-high-resolution mass spectra. Cartridge-extracted samples were diluted to approximately 500 mg/L with 1:1 methanol/water (v/v). Using a syringe pump at a flow rate of 120 $\mu L \cdot h^{-1}$, the diluted sample was injected into the ESI unit with a voltage of –3.8 kV. An equilibrium time of 0.06 s was set to allow ion accumulation in the hexapole ion trap prior to injection into the ICR cell. A broadband mass scan ranging from 100–1000 Da was conducted, and a total of 200 mass spectra were accumulated per sample. Duplicate measurements were collected for each sample to ensure reproducibility and reliability. The injection syringe and lines were rinsed three times with a 1:1 methanol/water (v/v) solution between each sample injection. A blank sample (i.e., NOM-free acidified ultrapure water) was extracted and analyzed to exclude any signal interferences. Further information on data analysis was provided in SI (Text S1e–g).

2.4 Complementary analysis

A Cary 60 spectrophotometer (Agilent, USA) was used to measure the UV light absorbance of the NOM solutions at 254 nm (UV_{254}). The total organic carbon concentration of the NOM solution was analysed with a Shimadzu TOC-L analyzer (SHIDMAZU, Japan). The EDC of NOM samples was measured using a size exclusion chromatography (SEC) coupled with a post-column reaction unit and two UV detectors, as previously reported [23]. *p*CBA and NB concentrations were measured with an HPLC unit equipped with a 250 mm × 4.6 mm C18 5-µm reverse phase column (AlltimaTM, GRACE) and UV detector (Agilent 1100 series, USA) by recording their absorbances at 238 nm and 270 mm, respectively.

3. Results and discussion

Fig. 1.

3.1 Reactivity of NOM isolates with radicals

Due to the selectivity of $SO_4^{\bullet-}$ to the chromophoric electron-rich moieties (i.e., aromatic or phenolic structures [29]), the time-dependent change in UV_{254} of the NOM samples was followed (at pH ~5) to compare their reactivity between the two radicals. To test the influence of pH on reactivity, the time-dependent UV_{254} decrease in a pH ~8 borate buffer solution was also measured. It was found that UV_{254} depletion became 10–20% less efficient at lower pH (i.e., ~5) for both UV/H_2O_2 and UV/PDS processes (Fig. S3). This finding indicated a probable inhibitory effect of a proton-rich environment on the NOM reactivity. This could be attributed to the protonation of some molecular structures at lower pH, leading to a lower reactivity compared with the deprotonated counterparts [30, 31]. However, the comparison between $^{\bullet}OH$ and $SO_4^{\bullet-}$ reactivity remains valid understanding that the experiments were conducted at similar pH i.e., similar NOM conformation and protonation character. It can be noted that the absolute reactivity reported in the current study (at pH ~5) might need correction when applied in other pH conditions.

At a reaction time of 30 min and for all three NOM isolates (Fig. 1a and Fig. S4), the decrease in UV_{254} was in average 22% higher following $SO_4^{\bullet-}$ oxidation as compared to that of $^{\bullet}OH$, probably due to the higher production yield of $SO_4^{\bullet-}$ under identical experimental conditions (Table S3). To validate a comparison in reactivity, the second-order rate constants (k_{sec}) of the chromophores were investigated considering the quantity of radicals produced and using the approach previously reported by Zhang et al. [23]. Specifically, the rate constants were calculated using the pseudo-first-order rate constants of UV_{254} decay (Table S3) and steady-state radical concentration (Table S3). A higher k_{sec} ($10^8\ M^{-1}s^{-1}$) was obtained for $^{\bullet}OH$ than for $SO_4^{\bullet-}$, i.e., 3.95 vs. 2.90, 7.37 vs. 2.12, and 4.30 vs. 1.20 for S-HPOA, R-HPO, and C-HPO, respectively (Fig. 1b and Fig. S4). These k_{sec} values for $SO_4^{\bullet-}$ might be slightly overestimated due to the presence of $^{\bullet}OH$ (i.e., calculated as <10% based on Text S1d) in the UV/PDS system. Moreover, the difference in the chromophores' reactivity between the

radicals varied among different NOM isolates. Specifically, the k_{sec} of $^{\bullet}OH$ was calculated as 1.4, 3.5, and 3.6-fold of that of $SO_4^{\bullet-}$ for S-HPOA, R-HPO, and C-HPO, respectively. In agreement with previous findings [23], the reactivity with $SO_4^{\bullet-}$ increased with the SUVA of untreated NOM samples (Text S2 and Table S1). However, no such correlation could be established for $^{\bullet}OH$, indicating the influence of other characteristics besides aromaticity. Interestingly, the TOC removal was negligible with $^{\bullet}OH$ oxidation (~10%) within 30 min, while a removal efficiency of approximately 35%, 48%, 43% for S-HPOA, R-HPO, and C-HPO, respectively, was achieved with $SO_4^{\bullet-}$ oxidation (Fig. S5).To further examine the different reactivity of these two radical species, a molecular-level investigation was conducted for NOM samples with a reaction time of 30 min using FT-ICR MS.

Fig. 2.

3.2 Identification of reactive molecules

The molecular formulas assigned through FT-ICR MS analysis for the untreated and the oxidized NOM fractions were compared. Based on previous studies [32, 33], the radical-reactive molecules were defined as those formulas disappearing after reaction and radical-resistant molecules were those remaining unchanged after reaction. Note that the molecular structures lost as TOC during the SPE extraction following oxidation (e.g., with the extraction efficiency decreasing from ~90% for the original S-HPOA to ~67% for its oxidized sample) were taken into account as radical reactive moieties. Moreover, the pool of reactive molecules could be underestimated, as the abated yet not eliminated molecules were not counted. In fact, it is impracticable to identify these molecules because the MS peak intensity could not be used for quantification. For instance, a higher (10–50%) total peak intensity was observed in the oxidized samples than the original NOMs in the current work, probably due to the breakdown of larger molecules and consequently a decreased suppression

effect [34]. In this regard, a partially oxidized molecule expected to generate a lower signal exhibited even higher peak intensity, leaving the identification of these molecules unobtainable. Further investigation on this analytical technique is still needed to achieve quantification. However, our findings based on this definition agreed well with the transformation of simple compounds, e.g., phenol and other substituted aromatics [5, 26, 35-39], as will be discussed in the following sections.

3.2.1 Categories of reactive molecules

Approximately 40%–50% of the total assigned formulas were identified as reactive (Table S4). To focus on the $^{\bullet}OH$ or $SO_4^{\bullet-}$ reaction, the contribution by direct UV photolysis was not considered by subtracting molecules found reactive to sole UV irradiation from the group of molecules reactive in UV/H_2O_2 or UV/PDS system. UV-reactive molecules accounted for ~ 27% of the total reactive molecules in UV/H_2O_2 or UV/PDS process (Table S4). Interestingly, although the UV-reactive molecules were characterized as large in size and rich in electrons, a transformation pathway different from radical oxidation was observed, which will be reported in a separate work. The distribution of the reactive and resistant molecules was visualized in van Krevelen diagrams based on their respective H/C and O/C ratios (Fig. 2). As shown in Fig. 2a and 2c, the majority of the reactive molecules within S-HPOA were assigned to lignins/carboxyl-rich alicyclic moieties (CRAM)-like structures, accounting for 83% and 82% in $^{\bullet}OH$- and $SO_4^{\bullet-}$-based AOPs, respectively. Similar results were also obtained with R-HPO and C-HPO (Fig. S6 and S7). Interestingly, higher removal efficiency (i.e., the ratio of the number of reactive molecules to that of total molecules of a specific category) (Table S5) was observed for aromatics and lignins/CRAM-like structures with $SO_4^{\bullet-}$ oxidation, and was consistent with the recorded higher decrease in UV_{254} (Fig. 1). The results were also in good agreement with the previous findings pertaining to the selectivity of $SO_4^{\bullet-}$ to aromatic moieties [8, 23].

3.2.2 Molecular characteristics of reactive molecules

To determine the influence of other NOM characteristics on its reactivy, the weight-averaged values (eq. S6–S7, SI) for various molecular characteristics (i.e., m/z_{wa}, DBE_{wa}, H/C_{wa}, and O/C_{wa}) between reactive and resistant molecules were calculated and compared (Table S6). These parameters were selected because they could reflect specific properties of NOM [32, 33], for instance, degree of unsaturation (DBE, H/C), molecular size (m/z), and degree of oxygenation (O/C). Moreover, their alteration upon oxidation could indicate the possible transformation pathways. The reactive molecules exhibited higher m/z_{wa}, C_{wa}, and DBE_{wa}, but lower H/C_{wa} and O/C_{wa} as compared to resistant molecules (Table S6). Overall, the results indicated that larger molecules with a higher degree of unsaturation and electron density were more susceptible to $^{\bullet}OH$ and $SO_4^{\bullet-}$ attacks. The higher reactivity of electron-rich molecules to radicals has also been observed among phenolic compounds and NOM [4, 5, 23, 26, 37, 38]. Specifically, the DBE_{wa} of $SO_4^{\bullet-}$ reactive molecules was the highest for S-HPOA (14.69, Table S6), also exhibiting the highest reactivity. The lowest DBE_{wa} of $SO_4^{\bullet-}$ reactive molecules was observed with C-HPO (11.55, Table S6), also associated with the lowest reactivity (Fig. 1). Interestingly, the molecules of S-HPOA reactive to $^{\bullet}OH$ were characterized by the highest DBE_{wa} (Table S6); however, the rate constant of the reaction between $^{\bullet}OH$ and S-HPOA was the lowest among the three NOM isolates (Fig. 1). The highest reactivity was observed with R-HPO (Fig. 1), showing a medium DBE_{wa} value for the reactive molecules (Table S6). This result is probably associated with the molecular size of the reactive molecules within R-HPO; for instance, the m/z_{wa} (481.06) and C_{wa} (22.99) values of its reactive molecules were the lowest as compared to S-HPOA (537.65/26.13) or C-HPO (518.13/25.18) (Table S6). The correlation between the reactivity of NOM fractions and molecular size has been previously documented [39], where the reactivity increased with decreasing molecular size. The critical role of electron density in $SO_4^{\bullet-}$ reaction could explain

the different reactivity observed among the three NOM isolates in Fig. 1a and Fig. S4, which is correlated with the initial DBE_{wa} values (Table S2).

3.2.3 N- or S-content of reactive molecules

The reactive and resistant molecules were also plotted based on their molecular composition, i.e., CHO, CHON, CHOS, and CHONS (Fig. 2b and 2d). Molecules containing only CHO (an average removal efficiency of 39%) were less reactive than those also containing N and S (an average removal efficiency of 44%, 59%, and 100% for CHON, CHOS, and CHONS, respectively). This trend was further confirmed by a similar observation for the two N- or S-enriched NOM isolates, i.e., R-HPO and C-HPO (Fig. S6 and S7). Consistent with previous findings [8], these results indicated that molecules incorporating N- or S-containing functional groups (e.g., $–NH_2$, –NH–, or –S–) are more reactive to both radical species [26, 37]. However, the difference in the reactivity of these molecules between $^{\bullet}OH$ and $SO_4^{\bullet-}$ was not significant, i.e, S-HPOA (6% vs. 6%), R-HPO (47% vs. 45%), and C-HPO (37% vs. 33%) (Table S7). The increased reactivity caused by the presence of S or N would explain the observed trend in $^{\bullet}OH$-induced reactivity (Fig. 1). Besides the influence of molecular size, the highest reactivity of R-HPO to $^{\bullet}OH$ could also be attributed to the largest fraction of N- or S-containing reactive molecules, accounting for approximately 47% (Text S2 and Table S7). Similarly, the lower reactivity of S-HPOA, as compared to C-HPO, could be a result of the lower content of N or S in its reactive molecules (6% vs. 37%, Table S7). Collectively, the results reflected that NOM reactivity towards $SO_4^{\bullet-}$ is highly dependent on the content of electron-rich moieties, while that of $^{\bullet}OH$ is also influenced by molecular size, non-oxygen heteroatom incorporation, and associated functional groups.

3.3 Exclusively reactive molecules

3.3.1 H/C

The molecules degraded by $^{\bullet}OH$ and $SO_4^{\bullet-}$ were compared to identify specific reactive sites. The molecules that only reacted with $^{\bullet}OH$ or $SO_4^{\bullet-}$ radicals accounted for approximately 10–20% of the total reactive molecules. The identification of these molecules was performed to assist in unraveling the distinct reaction pathways between the two radicals, as it will be discussed in Section 3.4. The H/C_{wa} of the molecules only reactive towards $^{\bullet}OH$ were higher than that of $SO_4^{\bullet-}$, with the largest difference observed with S-HPOA (1.11 vs. 0.86), medium difference with R-HPO (1.06 vs. 1.02), and smallest difference with C-HPO (1.03 vs. 1.02) (Table S8). This variation (i.e., the difference in the H/C_{wa} of exclusively reactive molecules) among different NOM isolates could probably be ascribed to the distinction in the initial H/C of the original samples (Table S2). For instance, the selection of molecules with higher H/C in R-HPO and C-HPO (i.e., with a H/C_{wa} of 1.11 and 1.19, respectively) by $SO_4^{\bullet-}$ would be with higher probability than S-HPOA (i.e., with a H/C_{wa} of 1.05). This would lead to a smaller difference between the H/C_{wa} of molecules uniquely reactive to $^{\bullet}OH$ and $SO_4^{\bullet-}$.

To further elucidate the difference in the H/C_{wa} of exclusively reactive molecules, the respective number of reactive molecules located in Area I (i.e., with higher H/C: 1.2–1.6 and lower O/C: 0.2–0.5, Fig. 3) were compared. Specifically, the percentage of molecules in Area I exclusively reactive towards $SO_4^{\bullet-}$ was only 19% for S-HPOA and 33% for C-HPO, respectively. Interestingly, the exclusively $SO_4^{\bullet-}$-reactive molecules were more abundant in this region for R-HPO (i.e., up to 63%, Fig. 3). However, the DBE_{wa} of the molecules exclusively reactive to $SO_4^{\bullet-}$ (9.54) in Area I was higher than that of $^{\bullet}OH$ (7.86). The observation is in agreement with the high affinity of $SO_4^{\bullet-}$ with electron-rich molecules. In addition, molecules exclusively reactive to $^{\bullet}OH$ falling in the same Area I were observed as more aliphatic, clearly indicated by their lower DBE_{wa} compared to the value determined for the total exclusively reactive molecules (i.e., 8.36 vs. 10.86, 7.86 vs. 11.06, and 6.69 vs. 10.47 for S-HPOA, R-HPO, and C-HPO respectively, Table S8).

Fig. 3.

3.3.2 O/C

The O/C_{wa} of molecules exclusively reactive to $SO_4^{\bullet-}$ was 10–22% higher than that of $^{\bullet}OH$, 0.55 vs. 0.45, 0.55 vs. 0.50, 0.52 vs. 0.47, for S-HPOA, R-HPO, and C-HPO respectively (Table S8). For instance, a larger fraction of molecules (i.e., 83%, 74%, and 75% for S-HPOA, R-HPO, and C-HPO, respectively) located in Area II (higher O/C: 0.5–0.7, and lower H/C: 0.7–1.2, Fig. 3) were observed to exclusively react with $SO_4^{\bullet-}$. Because the molecules were categorized as lignins/CRAM-like structures, one of the probable contributors to the higher O/C would be the carboxyl group (–COOH). Therefore, Kendrick Mass Defect (KMD) of homologous series with –COOH base [40], i.e., KMD (COO), were calculated (eq. S8-S10, SI) and plotted against the number of oxygen atoms (Fig. 4, Fig. S8). In these figures, molecules fall onto the same horizontal line belong to –COOH-based homologous series, with those on the right-hand side bearing more –COOH groups. As shown in Fig. 4 and Fig. S8, the majority of molecules exclusively reactive to $SO_4^{\bullet-}$ (green dots) distributed on the right of the KMD (COOH) vs. Oxygen number map, as compared to that of $^{\bullet}OH$. The results distinctly showed that molecules exclusively reactive to $SO_4^{\bullet-}$ presented a higher degree of –COOH functionalization than the $^{\bullet}OH$-reactive compounds.

Fig. 4.

3.3.3 DBE and molecular size

A higher value of DBE_{wa} was observed with molecules exclusively reactive to $SO_4^{\bullet-}$ as compared to those of $^{\bullet}OH$ (15.66 vs. 10.86, 11.86 vs. 11.06, and 11.53 vs. 10.47 for S-HPOA, R-HPO, and C-HPO, respectively) (Table S8). The difference in DBE was also illustrated in Fig. 5, Fig. S9, and S10, where DBE was plotted against the number of carbon atoms with reference to the O/C ratio. Specifically, the DBE of the vast majority of molecules exclusively reactive to $^{\bullet}OH$ was lower than the DBE_{wa} of the molecules exclusively reactive

towards $SO_4^{\bullet-}$ (i.e., 15.66 for S-HPOA), as illustrated by the black dash line in Fig. 5. Interestingly, the larger values of DBE (i.e., larger than 15.66 in Fig. 5b) were contributed by molecules with a larger number of carbon atoms (i.e., 20–37). Theoretically, the oxidation of $SO_4^{\bullet-}$ towards larger molecules (i.e., with a larger number of carbon atoms) was unfavorable due to the higher electrosteric repulsion phenomenon between the two [41, 42]. These findings demonstrated the critical role of electron density in $SO_4^{\bullet-}$ reaction (as reflected by DBE), where the high electron density of a molecule would counterbalance the steric repulsion and successfully trigger $SO_4^{\bullet-}$ oxidation. However, the unfavorable $^{\bullet}OH$ reaction with these molecules could probably be associated with its preferential radical addition pathway (as will be discussed in Section 3.4.3). Compared with SET to $SO_4^{\bullet-}$, $^{\bullet}OH$ addition might be more affected by the molecular size of NOM molecules, because $^{\bullet}OH$ oxidation may have less chance to occur with large molecules (as discussed in Section 3.2.2).

Fig. 5.

3.4 Reaction pathways

3.4.1 H-abstraction by $^{\bullet}OH$

The results in Section 3.3.1 indicated the intrinsic difference in reactive sites between the two radicals regardless of radical concentrations. Specifically, $[SO_4^{\bullet-}]_{ss}$ was higher than $[^{\bullet}OH]_{ss}$ (Table S3) under identical experimental conditions arising from the higher quantum yield of PDS than H_2O_2 [12]. Due to a negligible carbon removal (Fig. S5), a reaction pathway of H-abstraction [19] would be highly possible following the preferential targeting of these more aliphatic structures (i.e., molecules with higher H/C ratio and lower DBE) by $^{\bullet}OH$. Consistently, H-abstraction has been reported to be more spontaneous (i.e., with lower energy barrier) in the reaction of phenols with $^{\bullet}OH$ than $SO_4^{\bullet-}$ [5]. To test this hypothesis, the change in the H/C_{wa} of the produced molecules was also investigated. The produced molecules were

only those extractable with SPE, partially representing the complete pool of produced species due to a decreased extraction efficiency following radical oxidation (i.e., 89%, 78%, and 56% for untreated S-HPOA, $^{\bullet}OH$ and $SO_4^{\bullet-}$ treated samples, respectively). The newly formed molecules were characterized by a 5–10% lower H/C_{wa} (Table S9) in the $^{\bullet}OH$ oxidation system as compared to that in the $SO_4^{\bullet-}$ oxidation system. This observation is supporting the hypothesis of a more prevalent H-abstraction from NOM molecules by $^{\bullet}OH$ than $SO_4^{\bullet-}$.

3.4.2 Decarboxylation by $SO_4^{\bullet-}$

The preferential targeting of carboxyl-rich molecules by $SO_4^{\bullet-}$ (Section 3.3.2) originated from its favorable (i.e., spontaneous) single electron transfer (SET) reaction pathways [26]. SET from these molecules to $SO_4^{\bullet-}$would cause the production of cationic species as intermediates, which were stabilized with the leaving of –COOH (i.e., decarboxylation) [43]. However, as SET between $^{\bullet}OH$ and the carboxylated molecules was reported to be less favorable [26], the SET-initiated decarboxylation would not occur in $^{\bullet}OH$ process. In fact, $^{\bullet}OH$ would predominantly react through radical addition (as will be confirmed in Section 3.4.3), leading to the generation of numerous hydroxylated, oxygenated, or ring-cleavage products (i.e, no carbon removal) [44]. This would consequently lead to the observed negligible carbon removal (i.e., <10%) in $^{\bullet}OH$ process (Fig. S5). For the exclusively reactive sites, the faster H-abstraction by $^{\bullet}OH$ (10^8–10^9 $M^{-1}\cdot s^{-1}$) [45] than decarboxylation by $SO_4^{\bullet-}$(10^6–10^9 $M^{-1}\cdot s^{-1}$) [46] could explain the higher reactivity of NOM to $^{\bullet}OH$. Instead of a decrease in the O/C_{wa} of the extractable produced molecules highly expected due to decarboxylation, an increase was observed (Table S9). The observation is consistent with the large increase in O/C associated with a modest increase in H/C noted in the oxidation of simple aromatic compounds (Fig. S11). For instance, an O/C of 0.17 for phenol increased to 2.0 for formic acid. This increase could be attributed to the prevalence of hydroxylation and oxygenation in radical oxidation processes. Interestingly, the O/C_{wa} of extractable produced

molecules by $SO_4^{\bullet-}$ oxidation was even higher than that of $^{\bullet}OH$. The higher O/C_{wa} was observed to correlate with the assigned S-containing molecules, possibly formed through $SO_4^{\bullet-}$ addition [35]. However, further investigation is necessary to confirm this hypothesis. The molecular formula assignment remains a challenge in the analysis of FT-ICR MS data, especially with the inclusion of non-oxygen heteroatoms (i.e., S, N) and the increase of molecular mass [47, 48]. The investigation on the transformation of single model compound with $SO_4^{\bullet-}$ might be able to provide additional insights. The possible reaction pathway through $SO_4^{\bullet-}$ addition was not further discussed as not being the focus of this investigation.

3.4.3 $^{\bullet}OH$ addition and SET to $SO_4^{\bullet-}$

Since the exclusively reactive molecules only accounted for 10–20% of total reactive molecules, distinct reaction pathways associated with shared (major) reactive sites would also be expected to shape the different reactivity between NOM and the radicals. Therefore, the reaction pathways of the major reactive sites were explored in the following section. Lignins (i.e., as predominant reactive molecules in both reaction processes, Fig. 2a and 2c) have been reported as the primary contributors to both UV-light absorbing property and the electron-donating capacity (EDC) of NOM [49, 50]. The changes in EDC and UV_{254} (UV light absorbance at 254 nm) of the three NOM isolates were measured. Both EDC and UV_{254} values, in all three NOM isolates, were more efficiently depleted by $SO_4^{\bullet-}$ than $^{\bullet}OH$ (Fig. S12). To differentiate the reaction pathways, changes in EDC and UV_{254} were further explored by plotting the normalized EDC decrease versus the corresponding normalized UV_{254} decay (Fig. 6). In $^{\bullet}OH$-based AOPs, the EDC of R-HPO and C-HPO decreased slower than UV_{254}; contrariwise, a slightly faster decrease in EDC was observed for S-HPOA (Fig. 6a). Interestingly, a faster decrease in EDC than in UV_{254} was recorded with all three NOM isolates in $SO_4^{\bullet-}$-based AOPs (Fig. 6b).

The discrepancy in the EDC-UV_{254} correlations between these radical-based AOPs indicated a difference in reaction pathways. Specifically, the $SO_4^{\bullet-}$ reaction was initiated with one electron transfer from phenolic –OH moieties leading to the oxidation of phenolic structures, while the UV light absorbing property was preserved [23]. The $^{\bullet}OH$ reaction would lead to the destruction of aromatic moieties; however, the preservation of phenolic structures probably involved a radical addition to non-phenolic aromatic moieties [51]. Consequently, the higher reaction rate of $^{\bullet}OH$ radical addition (diffusion-limited) [45] than electron transfer to $SO_4^{\bullet-}$ (10^6–10^9 $M^{-1}\cdot s^{-1}$) [46] would lead to the higher reactivity of NOM to $^{\bullet}OH$.

The slightly faster decrease of EDC than UVA_{254} observed with S-HPOA in the presence of $^{\bullet}OH$ (i.e., an opposite trend from R-HPO and C-HPO) was probably caused by its higher degree of aromatic substitution as suggested by the higher SUVA and EDC values (Table S1). As a consequence, the oxidation of phenolic structures would be predominant due to the lower available sites for radical addition. This result could also explain the smaller difference in the reactivity between $^{\bullet}OH$ and $SO_4^{\bullet-}$ for S-HPOA as compare to R-HPO or C-HPO (Fig. 1).

Fig. 6.

4. Conclusions, implications, and future perspectives.

The second-order rate constant of chromophoric NOM was calculated as higher with $^{\bullet}OH$ than $SO_4^{\bullet-}$ based on the time-dependent UV_{254} decay and steady-state radical concentration. The rate constants with $SO_4^{\bullet-}$ were positively correlated with the SUVA values of the initial NOM samples, which was not observed in the $^{\bullet}OH$ process. FT-ICR MS analysis supported the predominant role of electron density (i.e., DBE) in $SO_4^{\bullet-}$ process, while the reactivity towards $^{\bullet}OH$ could also be affected by molecular size (i.e., *m/z*) and molecular composition (i.e., N- or S- incorporation). Identification of exclusively $^{\bullet}OH$- and $SO_4^{\bullet-}$- reactive molecules (i.e., taking up to 10–20% of the total reactive pool) reveal the preferential H-abstraction

(10^8–10^9 $M^{-1}\cdot s^{-1}$) by $^{\bullet}OH$ and decarboxylation by $SO_4^{\bullet-}$ (10^6–10^9 $M^{-1}\cdot s^{-1}$). Moreover, the reaction pathways associated with the shared reactive molecules (80–90%) were also found dissimilar based on EDC analysis, with radical addition (diffusion-limited) being predominant with $^{\bullet}OH$ while SET (10^6–10^9 $M^{-1}\cdot s^{-1}$) favorable with $SO_4^{\bullet-}$. The faster $^{\bullet}OH$-initiated reaction associated with the reactive sites (i.e., both exclusive and shared) explained the observed higher reactivity (i.e., second-order rate constant).

Understanding the reactivity and transformation of NOM in $^{\bullet}OH$ or $SO_4^{\bullet-}$-based process is useful to predict its behavior in engineered and natural aquatic systems. For instance, the reactivity of a specific NOM could be evaluated based on its molecular characteristics. The photoreactivity of NOM could be decreased after reaction with $^{\bullet}OH$ or $SO_4^{\bullet-}$ because molecules with higher DBE (i.e., which are preferentially degraded) were reported as more photosusceptible [28]. A proper radical-based treatment strategy for the degradation of target sites in complex organic matrices could be more efficiently implemented. For example, $SO_4^{\bullet-}$-based oxidation process could be adopted for the decrease of carboxyl-rich molecules (e.g., removal of membrane foulants [52]) because of its observed higher affinity to –COOH; while $^{\bullet}OH$-based oxidation process could be selected for the removal of organics with abundant aliphatic structures.

The structures of the molecules are yet to be confirmed, although their formulas have been unambiguously assigned. More complex water matrices representing natural waters (i.e., containing Cl^-, HCO_3^-, or varying pH conditions) should also be considered in future studies. The current study clearly showed the role of NOM character in controlling the radical-based reactions, a correlation between reactivity and characteristics using a larger pool of NOM isolates (i.e., various origins and molecular composition) could be established for a more accurate and convenient prediction of its reactivity in future work.

Acknowledgments

The authors would like to thank the China Scholarship Council (CSC) and Curtin University for providing a joint CSC-Curtin postgraduate scholarship to Suona Zhang. Dr. Valentin Rougé was also acknowledged for valuable help in EDC analysis.

References

1. Xie, P., et al., *Removal of 2-MIB and geosmin using UV/persulfate: Contributions of hydroxyl and sulfate radicals.* Water Research, 2015. **69**: p. 223-233.

2. Yang, W., H. Zhou, and N. Cicek, *Treatment of Organic Micropollutants in Water and Wastewater by UV-Based Processes: A Literature Review.* Critical Reviews in Environmental Science and Technology, 2014. **44**(13): p. 1443-1476.

3. Miklos, D.B., et al., *UV/H_2O_2 process stability and pilot-scale validation for trace organic chemical removal from wastewater treatment plant effluents.* Water Research, 2018. **136**: p. 169-179.

4. Nihemaiti, M., et al., *Removal of trace organic chemicals in wastewater effluent by UV/H_2O_2 and UV/PDS.* Water Research, 2018. **145**: p. 487-497.

5. Mei, Q., et al., *Sulfate and hydroxyl radicals-initiated degradation reaction on phenolic contaminants in the aqueous phase: Mechanisms, kinetics and toxicity assessment.* Chemical Engineering Journal, 2019. **373**: p. 668-676.

6. Sun, Y., et al., *Degradation of antibiotics by modified vacuum-UV based processes: Mechanistic consequences of H_2O_2 and $K_2S_2O_8$ in the presence of halide ions.* Science of The Total Environment, 2019. **664**: p. 312-321.

7. Sarathy, S.R., *Effects of UV/H_2O_2 advanced oxidation on physical and chemical characteristics of natural organic matter in raw drinking water sources*. 2009.

8. Varanasi, L., et al., *Transformations of dissolved organic matter induced by UV photolysis, Hydroxyl radicals, chlorine radicals, and sulfate radicals in aqueous-phase UV-Based advanced oxidation processes.* Water Research, 2018. **135**: p. 22-30.

9. Guo, L., et al., *Heterogeneity of natural organic matter from the Chena River, Alaska.* Water Research, 2003. **37**(5): p. 1015-1022.

10. Zafiriou, O.C., et al., *Photochemistry of natural waters.* Environmental Science & Technology, 1984. **18**(12): p. 358A-371A.

11. Cabaniss, S.E., *Forward Modeling of Metal Complexation by NOM: II. Prediction of Binding Site Properties.* Environmental Science & Technology, 2011. **45**(8): p. 3202-3209.

12. Autin, O., et al., *The impact of background organic matter and alkalinity on the degradation of the pesticide metaldehyde by two advanced oxidation processes: UV/H_2O_2 and UV/TiO_2.* Water Research, 2013. **47**(6): p. 2041-2049.

13. Guan, Y.-H., et al., *Efficient degradation of atrazine by magnetic porous copper ferrite catalyzed peroxymonosulfate oxidation via the formation of hydroxyl and sulfate radicals.* Water Research, 2013. **47**(14): p. 5431-5438.

14. Lee, N., G. Amy, and J.-P. Croué, *Low-pressure membrane (MF/UF) fouling associated with allochthonous versus autochthonous natural organic matter.* Water Research, 2006. **40**(12): p. 2357-2368.

15. Lee, N., et al., *Morphological analyses of natural organic matter (NOM) fouling of low-pressure membranes (MF/UF).* Journal of Membrane Science, 2005. **261**(1): p. 7-16.

16. Croué, J.-P., D. Violleau, and L. Labouyrie. *Disinfection by-product formation potentials of hydrophobic and hydrophilic natural organic matter fractions: a comparison between a low-and a high-humic water.* in *ACS Symposium Series*. 2000. Washington, DC; American Chemical Society; 1999.

17. Le Roux, J., M. Nihemaiti, and J.-P. Croué, *The role of aromatic precursors in the formation of haloacetamides by chloramination of dissolved organic matter.* Water Research, 2016. **88**: p. 371-379.

18. Hem, L.J. and H. Efraimsen, *Assimilable organic carbon in molecular weight fractions of natural organic matter.* Water Research, 2001. **35**(4): p. 1106-1110.

19. Westerhoff, P., et al., *Electron Pulse Radiolysis Determination of Hydroxyl Radical Rate Constants with Suwannee River Fulvic Acid and Other Dissolved Organic Matter Isolates.* Environmental Science & Technology, 2007. **41**(13): p. 4640-4646.

20. Lutze, H.V., et al., *Degradation of Chlorotriazine Pesticides by Sulfate Radicals and the Influence of Organic Matter.* Environmental Science & Technology, 2015. **49**(3): p. 1673-1680.

21. Madhavan, V., H. Levanon, and P. Neta, *Decarboxylation by $SO_4^{\cdot-}$ Radicals.* Radiation Research, 1978. **76**(1): p. 15-22.

22. Sarathy, S. and M. Mohseni, *The fate of natural organic matter during UV/H_2O_2 advanced oxidation of drinking water.* Canadian Journal of Civil Engineering, 2008. **36**(1): p. 160-169.

23. Zhang, S., et al., *Reactivity of chromophoric dissolved organic matter (CDOM) to sulfate radicals: Reaction kinetics and structural transformation.* Water Research, 2019. **163**: p. 114846.

24. Lavonen, E.E., et al., *Tracking changes in the optical properties and molecular composition of dissolved organic matter during drinking water production.* Water Research, 2015. **85**: p. 286-294.

25. Zhang, H., et al., *Study on Transformation of Natural Organic Matter in Source Water during Chlorination and Its Chlorinated Products using Ultrahigh Resolution Mass Spectrometry.* Environmental Science & Technology, 2012. **46**(8): p. 4396-4402.

26. Luo, S., et al., *Quantitative structure–activity relationships for reactivities of sulfate and hydroxyl radicals with aromatic contaminants through single–electron transfer pathway.* Journal of Hazardous Materials, 2018. **344**: p. 1165-1173.

27. Lv, J., et al., *Molecular transformation of natural and anthropogenic dissolved organic matter under photo-irradiation in the presence of nano TiO_2.* Water Research, 2017. **125**: p. 201-208.

28. Gonsior, M., et al., *Photochemically Induced Changes in Dissolved Organic Matter Identified by Ultrahigh Resolution Fourier Transform Ion Cyclotron Resonance Mass Spectrometry.* Environmental Science & Technology, 2009. **43**(3): p. 698-703.

29. Fichot, C.G., et al., *Predicting Dissolved Lignin Phenol Concentrations in the Coastal Ocean from Chromophoric Dissolved Organic Matter (CDOM) Absorption Coefficients.* Frontiers in Marine Science, 2016. **3**(7).

30. Benner, J. and T.A. Ternes, *Ozonation of Metoprolol: Elucidation of Oxidation Pathways and Major Oxidation Products.* Environmental Science & Technology, 2009. **43**(14): p. 5472-5480.

31. Muzolf, M., et al., *pH-Dependent Radical Scavenging Capacity of Green Tea Catechins.* Journal of Agricultural and Food Chemistry, 2008. **56**(3): p. 816-823.

32. Remucal, C.K., et al., *Molecular-Level Transformation of Dissolved Organic Matter during Oxidation by Ozone and Hydroxyl Radical.* Environmental Science & Technology, 2020. **54**(16): p. 10351-10360.

33. Yuan, Z., et al., *Molecular Insights into the Transformation of Dissolved Organic Matter in Landfill Leachate Concentrate during Biodegradation and Coagulation Processes Using ESI FT-ICR MS.* Environmental Science & Technology, 2017. **51**(14): p. 8110-8118.

34. Sterner, J.L., et al., *Signal suppression in electrospray ionization Fourier transform mass spectrometry of multi-component samples.* Journal of Mass Spectrometry, 2000. **35**(3): p. 385-391.

35. Van Buren, J., et al., *Ring-Cleavage Products Produced during the Initial Phase of Oxidative Treatment of Alkyl-Substituted Aromatic Compounds.* Environmental Science & Technology, 2020.

36. Olmez-Hanci, T. and I. Arslan-Alaton, *Comparison of sulfate and hydroxyl radical based advanced oxidation of phenol.* Chemical Engineering Journal, 2013. **224**: p. 10-16.

37. Ye, T., et al., *Chemical structure-based predictive model for the oxidation of trace organic contaminants by sulfate radical.* Water Research, 2017. **116**: p. 106-115.

38. Westerhoff, P., et al., *Relationships between the structure of natural organic matter and its reactivity towards molecular ozone and hydroxyl radicals.* Water Research, 1999. **33**(10): p. 2265-2276.

39. Dong, M.M., S.P. Mezyk, and F.L. Rosario-Ortiz, *Reactivity of Effluent Organic Matter (EfOM) with Hydroxyl Radical as a Function of Molecular Weight.* Environmental Science & Technology, 2010. **44**(15): p. 5714-5720.

40. Sleighter, R.L. and P.G. Hatcher, *The application of electrospray ionization coupled to ultrahigh resolution mass spectrometry for the molecular characterization of natural organic matter.* Journal of Mass Spectrometry, 2007. **42**(5): p. 559-574.

41. Baalousha, M., K. Afshinnia, and L. Guo, *Natural organic matter composition determines the molecular nature of silver nanomaterial-NOM corona.* Environmental Science: Nano, 2018. **5**(4): p. 868-881.

42. Shen, M.-H., et al., *Effects of molecular weight-dependent physicochemical heterogeneity of natural organic matter on the aggregation of fullerene nanoparticles in mono- and di-valent electrolyte solutions.* Water Research, 2015. **71**: p. 11-20.

43. Zemel, H. and R.W. Fessenden, *The mechanism of reaction of sulfate radical anion with some derivatives of benzoic acid.* The Journal of Physical Chemistry, 1978. **82**(25): p. 2670-2676.

44. Klein, G.W., et al., *Reaction of hydroxyl radicals with benzoic acid. Isomer distribution in the radical intermediates.* The Journal of Physical Chemistry, 1975. **79**(17): p. 1767-1774.

45. Buxton, G.V., et al., *Critical Review of rate constants for reactions of hydrated electrons, hydrogen atoms and hydroxyl radicals (OH/O⁻) in Aqueous Solution.* Journal of Physical and Chemical Reference Data, 1988. **17**(2): p. 513-886.

46. Neta, P., et al., *Rate constants and mechanism of reaction of sulfate radical anion with aromatic compounds.* Journal of the American Chemical Society, 1977. **99**(1): p. 163-164.

47. Herzsprung, P., et al., *Molecular formula assignment for dissolved organic matter (DOM) using high-field FT-ICR-MS: chemical perspective and validation of sulphur-rich organic components (CHOS) in pit lake samples.* Analytical and Bioanalytical Chemistry, 2016. **408**(10): p. 2461-2469.

48. Ohno, T. and P.E. Ohno, *Influence of heteroatom pre-selection on the molecular formula assignment of soil organic matter components determined by ultrahigh resolution mass spectrometry.* Analytical and Bioanalytical Chemistry, 2013. **405**(10): p. 3299-3306.

49. Aeschbacher, M., et al., *Antioxidant properties of humic substances.* Environmental science & technology, 2012. **46**(9): p. 4916-4925.

50. Wenk, J., et al., *Chemical Oxidation of Dissolved Organic Matter by Chlorine Dioxide, Chlorine, And Ozone: Effects on Its Optical and Antioxidant Properties.* Environmental Science & Technology, 2013. **47**(19): p. 11147-11156.

51. Neta, P. and R.W. Fessenden, *Hydroxyl radical reactions with phenols and anilines as studied by electron spin resonance.* The Journal of Physical Chemistry, 1974. **78**(5): p. 523-529.

52. Lin, C.-F., S.-H. Liu, and O.J. Hao, *Effect of functional groups of humic substances on uf performance.* Water Research, 2001. **35**(10): p. 2395-2402.

Figure captions

Fig. 1. (a) UV_{254} decrease of S-HPOA with time, and (b) second-order rate constants (k_{sec}) of three NOM isolates with $^{\bullet}OH$ or $SO_4^{\bullet-}$. Conditions: Incident UV intensity = 0.9 $mW \cdot cm^{-2}$, $[TOC]_0$ = 3.89 ± 0.18 $mgC \cdot L^{-1}$, $[H_2O_2]_0$ or $[PDS]_0$ = 1.0 mM, at unadjusted pH ($[pH]_0$=4.65 ± 0.09) and room temperature (20°C). Note: The UV_{254} decrease of NOM samples through direct UV photolysis (3–11%) has been subtracted throughout the calculation.

Fig. 2. (a, c) van Krevelen diagrams and (b, d) molecular composition of S-HPOA after $^{\bullet}OH$ or $SO_4^{\bullet-}$ treatment. The olive points/bars represent the radical-reactive moieties (formulas that disappeared after reaction), and red points/bars reflect the radical-resistant structures (formulas remaining unchanged after reaction). Relative abundance indicates the ratio of the number of reactive or resistant molecules to the total number of molecules in each subgroup, i.e., CHO, CHON, CHOS, and CHONS.

Fig. 3. van Krevelen diagram of molecules exclusively reactive to $^{\bullet}OH$ or $SO_4^{\bullet-}$ within (a) S-HPOA, (b) R-HPO, and (c) C-HPO. Red points denote molecules exclusively reactive to $^{\bullet}OH$; while olive points denote molecules exclusively reactive to $SO_4^{\bullet-}$.

Fig. 4. KMD (COO) of molecules exclusively reactive with $^{\bullet}OH$ or $SO_4^{\bullet-}$ as a function of oxygen number in the NOM isolate of S-HPOA. The selected molecular formulas were presented as an illustration.

Fig. 5. DBE of molecules exclusively reactive to (a) $^{\bullet}OH$ or (b) or $SO_4^{\bullet-}$ as a function of number of carbon atoms based on O/C in S-HPOA. The dashed line indicates the comparison at a DBE value of 15.66 (DBE_{wa} of the molecules exclusively reactive to $SO_4^{\bullet-}$)

Fig. 6. Relationship between normalized UVA_{254} and EDC decrease of different NOM isolates in (a) $^{\bullet}OH$ and or (b) $SO_4^{\bullet-}$ reaction processes. Conditions: Incident UV intensity = 0.9 $mW \cdot cm^{-2}$, $[TOC]_0$ = 3.89 ± 0.18 $mgC \cdot L^{-1}$, and $[H_2O_2]_0$ or $[PDS]_0$ = 0.00–0.10 mM, at unadjusted pH (4.65 ± 0.09) and room temperature (20°C).

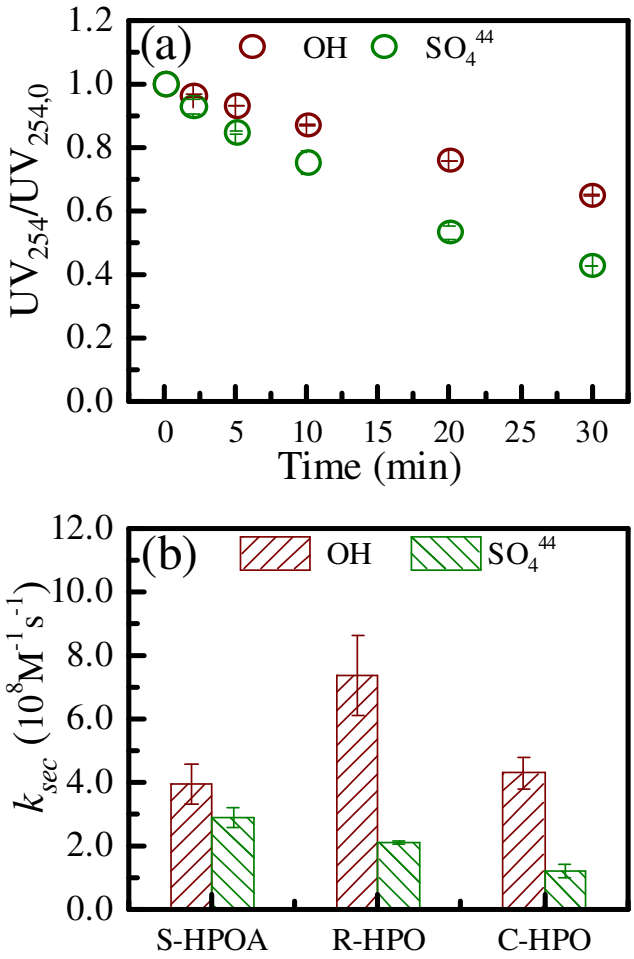

Fig. 1. (a) UV_{254} decrease of S-HPOA with time, and (b) second-order rate constants (k_{sec}) of three NOM isolates with $^{\bullet}OH$ or $SO_4^{\bullet-}$. Conditions: Incident UV intensity = 0.9 mW·cm^{-2}, $[TOC]_0$ = 3.89 ± 0.18 mgC·L^{-1}, $[H_2O_2]_0$ or $[PDS]_0$ = 1.0 mM, at unadjusted pH ($[pH]_0$=4.65 ± 0.09) and room temperature (20°C). Note: The UV_{254} decrease of NOM samples through direct UV photolysis (3–11%) has been subtracted in Fig.1a..

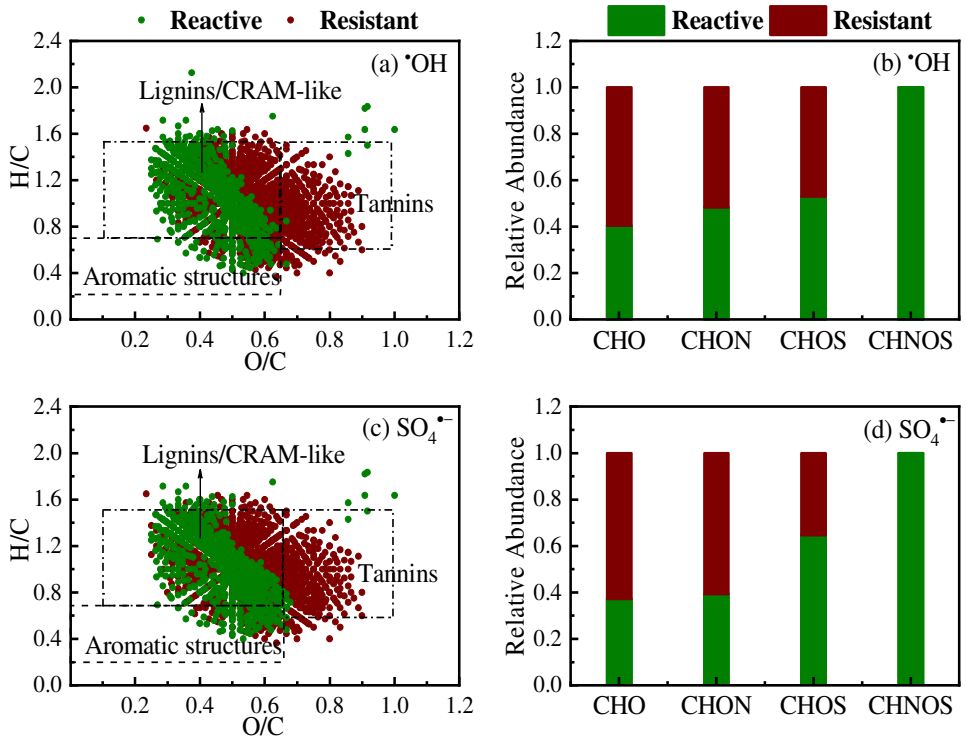

Fig. 2. (a, c) van Krevelen diagrams and (b, d) molecular compositions of S-HPOA after •OH or $SO_4^{\bullet-}$ treatment. The olive points/bars represent the radical-reactive moieties (formulas that disappeared after reaction), and red points/bars reflect the radical-resistant structures (formulas remaining unchanged after reaction). Relative abundance indicates the ratio of the number of reactive or resistant molecules to the total number of molecules in each subgroup, i.e., CHO, CHON, CHOS, and CHONS.

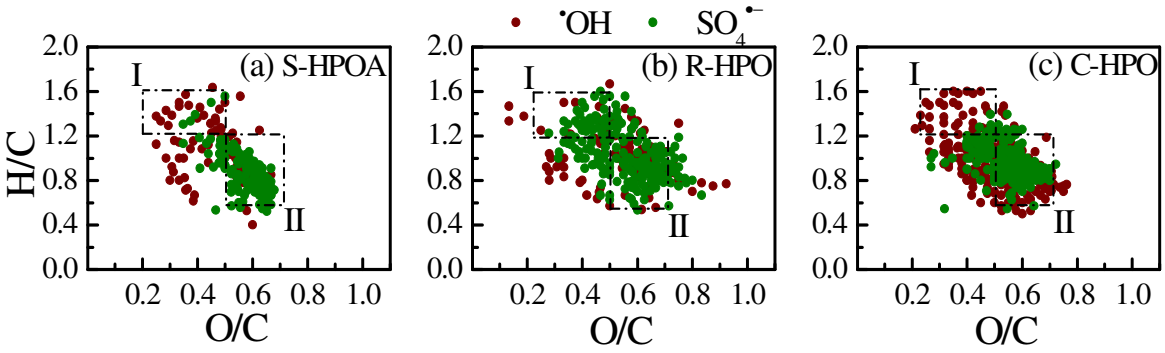

Fig. 3. van Krevelen diagram of molecules exclusively reactive to •OH or $SO_4^{\bullet-}$ within (a) S-HPOA, (b) R-HPO, and (c) C-HPO. Red points denote molecules exclusively reactive to •OH; while olive points denote molecules exclusively reactive to $SO_4^{\bullet-}$.

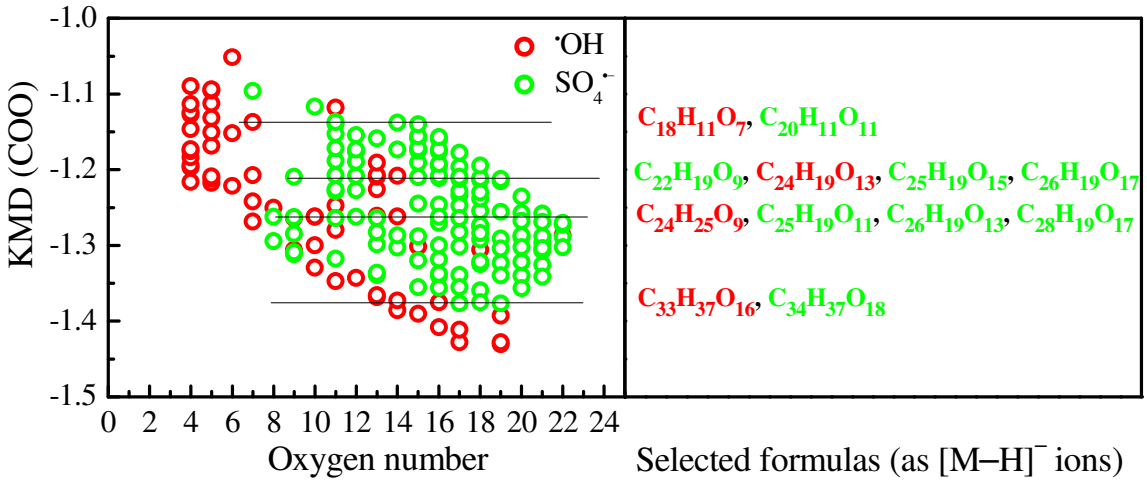

Fig. 4. KMD (COO) of molecules exclusively reactive with ·OH or $SO_4^{\bullet-}$ as a function of oxygen number in S-HPOA isolate. The selected molecular formulas were presented as an illustration.

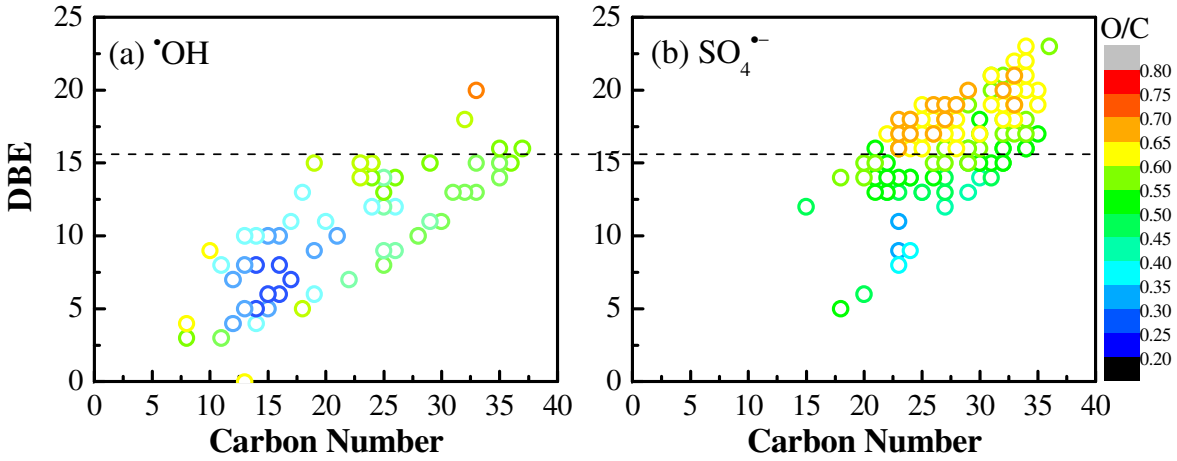

Fig. 5. DBE of molecules exclusively reactive to (a) •OH or (b) or $SO_4^{\bullet-}$ as a function of the number of carbon atoms based on O/C in S-HPOA isolate. The dashed line indicates the comparison at a DBE value of 15.66 (DBE_{wa} of the molecules exclusively reactive to $SO_4^{\bullet-}$).

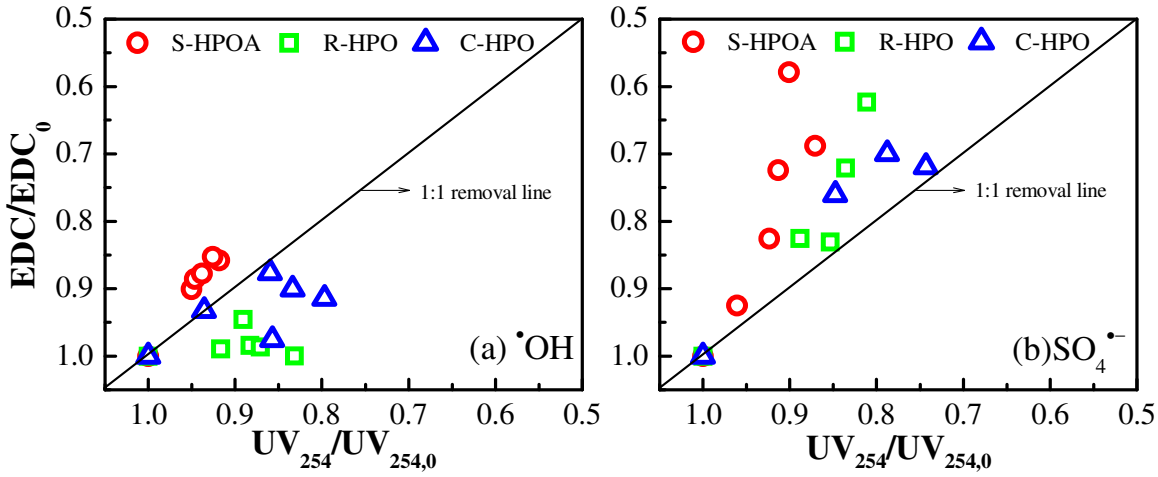

Fig. 6. Relationship between normalized UVA_{254} and EDC decrease of different NOM isolates in (a) $^{\bullet}OH$ and or (b) $SO_4^{\bullet-}$ reaction processes. Conditions: Incident UV intensity = 0.9 $mW \cdot cm^{-2}$, $[TOC]_0$ = 3.89 ± 0.18 $mgC \cdot L^{-1}$, and $[H_2O_2]_0$ or $[PDS]_0$ = 0.00–0.10 mM, at unadjusted pH (4.65 ± 0.09) and room temperature (20°C).

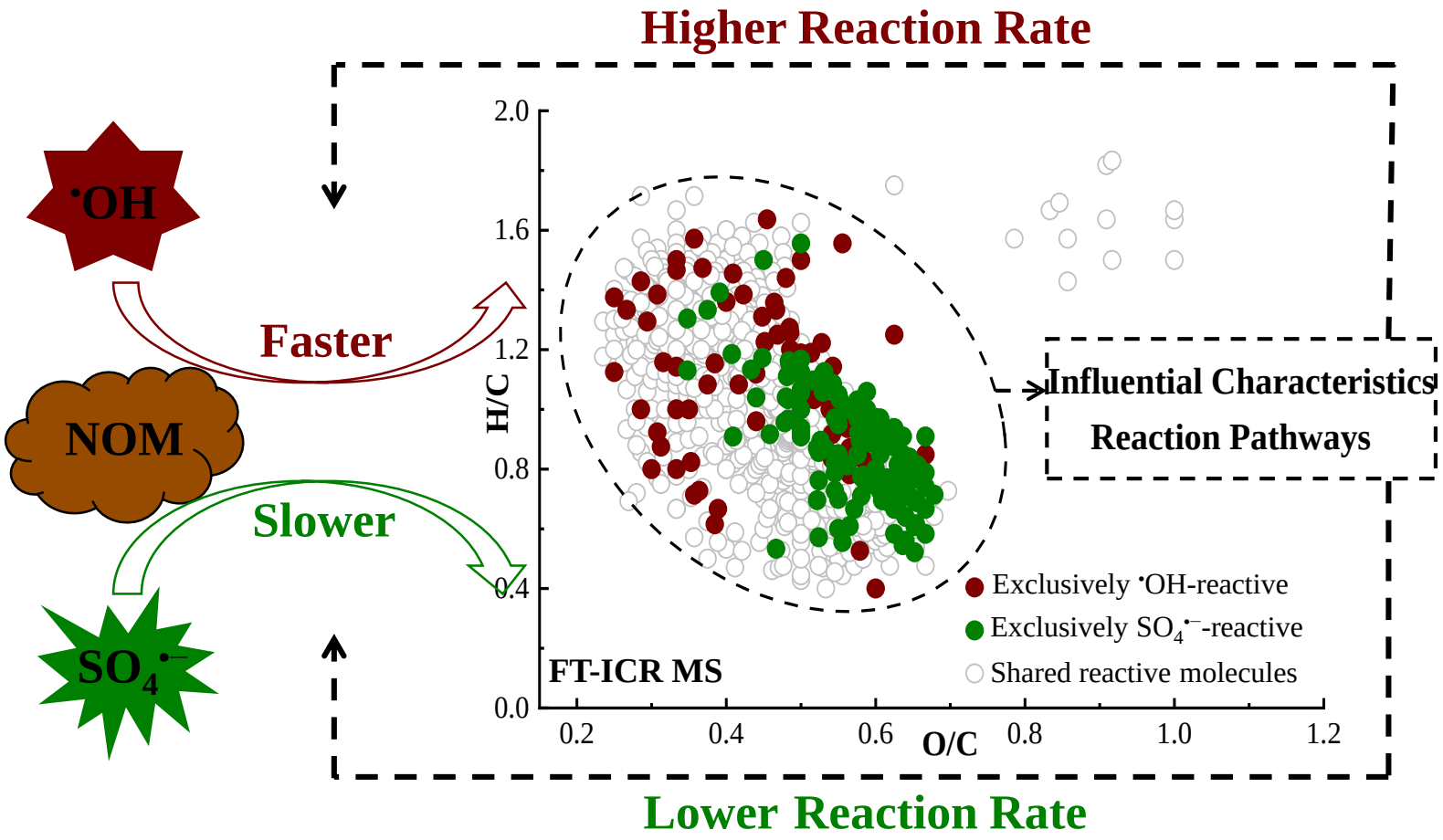
Higher Reaction Rate
·OH
Faster
NOM
Slower
SO4·−
2.0
1.6
1.2
0.8
0.4
0.0
H/C
0.2
0.4
0.6
0.8
1.0
1.2
O/C
FT-ICR MS
Exclusively ·OH-reactive
Exclusively SO4·−-reactive
Shared reactive molecules
Influential Characteristics
Reaction Pathways
Lower Reaction Rate